Original Article

MOLECULAR METABOLISM

Adipose tissue lipolysis is regulated by PAQR11 via altering protein stability of phosphodiesterase 4D

Meiqin Huang [1,3], Yijun Lin [1,3], Lin Wang [2], Xue You [1], Shuo Wang [1], Jingyu Zhao [1], Meijuan Bai [1], Zixuan Li [1], Yan Chen [1,*]

ABSTRACT

Fat storage and mobilization in adipose tissue play a central role in energy metabolism and are directly linked to the development of obesity. Upon starvation, fat is mobilized from adipose tissue by lipolysis, a process by which triglycerides are hydrolyzed to free fatty acids to be used as an energy source in skeletal muscles and other tissues. However, how lipolysis is activated by starvation is not fully known. In this study, we demonstrate that PAQR11, a member of the progesterone and AdipoQ receptor family, regulates starvation-mediated lipolysis. *Paqr11*-deleted mice are resistant to high-fat diet-induced obesity. *Paqr11* deletion promotes lipolysis in white adipose tissue, characterized by increased phosphorylations of hormone-sensitive lipase (HSL) and perilipin 1 (PLIN1) and elevated serum levels of glycerol and free fatty acids. PKA activity and cAMP levels in white adipose tissue are also increased by *Paqr11* deletion, accompanied by accelerated protein degradation of phosphodiesterase 4D (PDE4D). Mechanistically, PAQR11 decreases the interaction of PDE4D with SKP1-CUL1-FBXO2 E3 ligase complex, thus modulating the polyubiquitination/degradation of PDE4D. Fasting decreases the expression of the *Paqr11* gene, and starvation-induced lipolysis in white adipose tissue is enhanced by *Paqr11* deletion, while insulin-mediated suppression of lipolysis is not affected. Collectively, these results reveal that PAQR11 regulates lipolysis of adipose tissue and affects high-fat diet-induced obesity.

Keywords Lipolysis; Obesity; Ubiquitination; cAMP; PKA; PDE4D

1. INTRODUCTION

Storage and mobilization of triacylglycerol (TAG) in adipose tissue play a central role in energy metabolism and coordinate the feeding and fasting cycle of animals, including humans [1—3]. Upon feeding, the energy intake from fat is mainly reserved in the form of TAG in the adipose tissue, while the energy intake from carbohydrates is stored in the form of glycogen in the liver and skeletal muscle. The storage of TAG plays a more important role than glycogen for long-term energy reservation as fatty acid, the major component of TAG, contains the highest energy density among all energy substrates. In addition, a long-term increase in TAG storage directly leads to obesity, the most important health issue in modern society [4]. Therefore, a detailed understanding of TAG metabolism is key to combat obesity.

Catabolism of TAG is mainly achieved by a process called "neutral" lipolysis, while TAG in the lipid droplets of adipocytes is hydrolyzed by cytoplasmic lipases, in contrast to "acidic" lipolysis in which TAG is broken down in lysosomes [3]. For simplicity, lipolysis described in this study is limited to "neutral" lipolysis. Three sequential steps are needed to hydrolyze TAG into fatty acid and glycerol, catalyzed by three different enzymes. In the first step of this process, adipose triglyceride lipase (ATGL) hydrolyzes TAG to diacylglycerol (DAG). DAG is then hydrolyzed to monoacylglycerol (MAG) by hormone-sensitive lipase (HSL). In the last step, MAG lipase (MGL) converts MAG into fatty acids and glycerol [2,3]. Catecholamine-mediated regulation takes a center stage in the control of lipolysis. Activation of the sympathetic nervous system leads to elevation of catecholamines, including epinephrine and norepinephrine, which stimulates β-adrenergic receptors on the cell surface of adipocytes [5]. Activation of β-adrenergic receptors stimulates adenylyl cyclase (AC) and leads to an increase in intracellular cAMP and activation of protein kinase A (PKA) [6]. PKA activates lipolysis through phosphorylations of HSL and perilipin 1 (PLIN1) localized on the surface of lipid droplets, while phosphorylated PLIN1 releases CGI58 (comparative gene identification 58), which subsequently activates ATGL [7]. Activation of both HSL and ATGL thus turns on the lipolysis process of adipocytes.

In physiology, lipolysis is tightly coordinated with the feeding and fasting cycle of animals. Upon feeding, lipolysis is mainly inhibited by an anabolic hormone, *i.e.*, insulin. Insulin binds insulin receptors on the cell surface, leading to sequential activation of PI3K and AKT, which

[1]CAS Key Laboratory of Nutrition, Metabolism, and Food Safety, Shanghai Institute of Nutrition and Health, University of Chinese Academy of Sciences, Chinese Academy of Sciences, Shanghai, 200031, China [2]China Animal Health and Epidemiology Center, Qingdao, Shangdong, 266032, China

[3] Meiqin Huang and Yijun Lin contributed equally to this study.

*Corresponding author. E-mail: ychen3@sibs.ac.cn (Y. Chen).

Received December 27, 2020 • Revision received January 31, 2021 • Accepted February 1, 2021 • Available online 5 February 2021

https://doi.org/10.1016/j.molmet.2021.101182

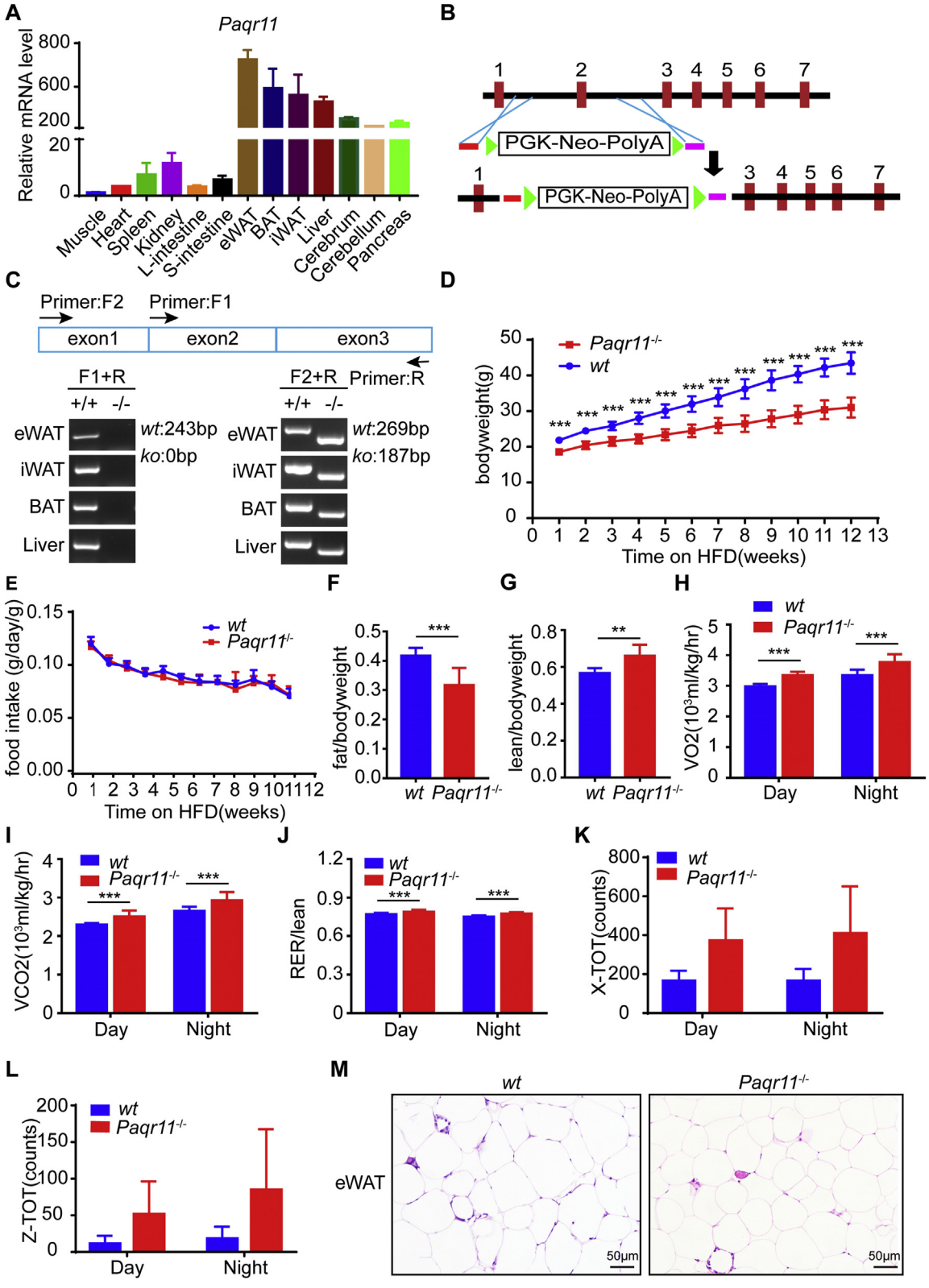

Figure 1: Deletion of *Paqr11* reduces HFD-induced obesity. (A) Quantitative RT-PCR analysis of RNA from various mouse tissues. (B) Schematic representation for generation of *Paqr11*$^{-/-}$ mice. (C) Genotyping of wild-type (*wt*) and *Paqr11*$^{-/-}$ mice in different tissues by PCR with genomic DNA. (D) Body weight gain in *wt* and *Paqr11*$^{-/-}$ mice fed with high-fat diet (HFD) for 3 months (male, HFD started at 6 weeks old, n = 8 for each group). (E) Food intake of the mice (normalized to body weight). (F, G) Body composition of the mice at the end of the experiment. (H, I, J) Oxygen consumption, carbon dioxide production and respiratory exchange ratio (RER) of the mice as measured during a 24-h period including a light cycle and a dark cycle. (K, L) Movement of the mice on the X and Z axes. (M) Representative images of H&E staining of eWAT (bar, 50 μm). All the quantitative data are shown as mean ± SD. * for $P < 0.05$, ** for $P < 0.01$, *** for $P < 0.001$.

phosphorylates phosphodiesterase 3B (PDE3B) and activates its activity, thus leading to breakdown of cAMP and shutdown of PKA-mediated lipolysis [8,9]. Although starvation is the primary physiological cue to initiate lipolysis, the underlying mechanism is still not fully understood [2]. Numerous theories have been proposed to explain how starvation activates lipolysis [2,3]. The long-held theory is that starvation stimulates the sympathetic nervous system that innervates the adipose tissue, leading to increase in systemic or local catecholamines, which activate β-adrenergic receptors [5,10]. In addition, many hormones and fasting-sensing molecules are hypothesized to be involved in starvation-induced lipolysis, such as glucagon [11], growth hormone [12], AMPK [13], mTOR [14], and SIRT1 [15]. Extensive studies with these factors significantly advanced our understanding about the complex regulation of lipolysis. However, these studies still do not completely elucidate how starvation turns on lipolysis [2]. For example, glucagon, a major hormone that elevates during starvation, cannot stimulate lipolysis at the physiological level [11]. In this study, we provide evidence that PAQR11, a member of the progesterone and adipoQ receptor family [16–18], plays a key role in linking starvation to lipolysis. Furthermore, the regulation of lipolysis by PAQR11 is associated with high fat diet-induced obesity, thus linking fasting-modulated lipolysis to the pathophysiology of obesity.

2. RESULTS

2.1. Deletion of *Paqr11* reduces HFD-induced obesity

As a member of the PAQR family, PAQR11 was previously reported to modulate Ras signaling and tumor cell migration/metastasis [17,18]. However, the physiological function of PAQR11 in mammals remains elusive. To understand the *in vivo* function of PAQR11, we first analyzed the tissue expression pattern of *Paqr11* in mice by reverse transcription-polymerase chain reaction (RT-PCR). *Paqr11* had the highest expression level among all analyzed adipose tissues, including epididymal adipose tissue (eWAT), inguinal adipose tissue (iWAT), and brown adipose tissue (BAT) (Figure 1A). We generated a systemic knockout of the *Paqr11* gene through a targeted disruption of murine *Paqr11* gene in the second exon by homologous recombination (Figure 1B). Deletion of *Paqr11* transcript was confirmed by RT-PCR using RNA isolated from both wild-type and *Paqr11*-deleted mouse tissues, including eWAT, iWAT, BAT, and livers (Figure 1C). As *Paqr11* is highly expressed in the adipose tissues, we next investigated whether *Paqr11* deletion impacted obesity. Upon feeding with a high-fat diet (HFD), $Paqr11^{-/-}$ mice gained body weight at a slower rate than the wild-type littermates (Figure 1D). The decreased body weight gain was also observed in $Paqr11^{-/-}$ mice fed a normal chow diet (SFigure 1A). There was no difference in food intake between the wild-type and $Paqr11^{-/-}$ mice (Figure 1E), indicating that the reduced obesity in $Paqr11^{-/-}$ mice under HFD was not caused by reduced food intake. Consistently, $Paqr11^{-/-}$ mice had a reduction in fat mass and an increase in lean mass compared with the wild-type mice (Figure 1F and G). Furthermore, $Paqr11^{-/-}$ mice fed HFD had increased oxygen consumption, carbon dioxide production, and respiratory exchange ratio (RER) (Figure 1H–J), but without significant changes in activities (Figure 1K and L). We also observed a similar metabolic phenotype with $Paqr11^{-/-}$ mice fed a normal chow diet (SFigure 1B–E). In addition, the size of adipocytes was smaller in the $Paqr11^{-/-}$ mice than in the wild-type mice in eWAT (Figure 1M), iWAT, and BAT (SFigure 2A). In addition, compared to the wild-type mice, $Paqr11^{-/-}$ mice had significant reductions in serum levels of total cholesterol (TC), low-density lipoprotein (LDL), and high-density lipoprotein (HDL) under the condition of HFD (SFigure 2B–E). However, glucose tolerance and insulin sensitivity were not altered in the $Paqr11^{-/-}$ mice (SFigure 2F and G). Collectively, these findings indicated that $Paqr11^{-/-}$ mice are both resistant to HFD-induced obesity and show an increase in metabolic rate.

2.2. Deletion of *Paqr11* increases lipolysis in adipose tissue

To explore the mechanism underlying the reduction of obesity in *Parq11*-deleted mice, we investigated whether lipolysis in adipose tissues was altered. We measured the mRNA levels of key lipolysis genes, including *Atgl*, *Hsl*, *Mgl*, and *Plin1,* and found that the expression of these genes was significantly elevated in the eWAT of overnight-fasted $Paqr11^{-/-}$ mice compared to that of the wild-type mice (Figure 2A). However, the expression of these genes was not altered in iWAT and BAT in the $Paqr11^{-/-}$ mice (SFigure 3A and B). The protein level of HSL was also increased in the eWAT of the $Paqr11^{-/-}$ mice (Figure 2B). More strikingly, phosphorylation of HSL was robustly elevated by *Paqr11* deletion (Figure 2B). The protein level of PLIN1 in eWAT was slightly increased by *Paqr11* deletion, while the phosphorylation of PLIN1 was markedly elevated in the $Paqr11^{-/-}$ mice (Figure 2C). Thus, these results indicated that *Paqr11* deletion increases fasting-induced lipolysis of eWAT through increasing expression of lipolysis genes and phosphorylation of HSL and PLIN1. We also analyzed HSL in iWAT and BAT and found that HSL phosphorylation was slightly elevated in iWAT but not BAT in the $Paqr11^{-/-}$ mice (SFigure 3C and D).

Consistent with the finding that *Paqr11* deletion elevated lipolysis of adipose tissue, serum levels of glycerol and free fatty acid (FFA) were increased in the overnight-fasted $Paqr11^{-/-}$ mice (Figure 2D and E). We also isolated primary mouse embryonic fibroblasts (MEFs) from the mice and differentiated them into adipocytes. The mRNA levels of *Atgl*, *Hsl*, *Mgl*, and *Plin1* were all elevated by *Paqr11* deletion in these cells (Figure 2F). Furthermore, phosphorylations of HSL and PLIN1 were markedly increased in *Paqr11*-deleted adipocytes (Figure 2G). The levels of glycerol and FFA in the cell culture medium of adipocytes were also increased by *Paqr11* deletion (Figure 2H and I). As the adipocytes were cultured in full medium without isoproterenol treatment, these data indicated that basal lipolysis is enhanced by *Paqr11* deletion.

In addition to lipolysis, we also analyzed a series of lipid metabolism-related markers in three adipose tissues of the mice. The major changes in eWAT were increases in markers of lipogenesis and lipid oxidation upon *Paqr11* deletion, without significant changes in markers of adipogenesis and browning (SFigure 4). Together with our results showing that lipolysis markers were also enhanced by *Paqr11* deletion, we postulate that the major function of *Paqr11* deletion in eWAT is to increase the turnover rate of lipid metabolism, with the net rate of lipid breakdown higher than that of lipid synthesis. In iWAT, there was an increase in markers of browning, but without change in markers of adipogenesis, lipid synthesis, and lipid oxidation (SFigure 4). These results suggested that *Paqr11* deletion mainly results in an increase of browning in iWAT, consistent with the findings that the size of adipocytes in iWAT was markedly decreased by *Paqr11* deletion (SFigure 2A) and the energy expenditure was increased in *Paqr11*-deleted mice (Figure 1H and I, SFigure 1B and C). In BAT, there was no significant changes in most of the lipid metabolism-related markers (SFigure 4). However, the size of adipocytes in BAT was reduced by *Paqr11* deletion (SFigure 2A). We postulate that such decrease in adipocyte size in BAT is likely an indirect result of the changes of lipid metabolism in the white adipose tissue as the latter comprises the most majority of adipose tissue in the body. Taken together, the major phenotypes of the *Paqr11*-deleted mice were an elevated turnover of

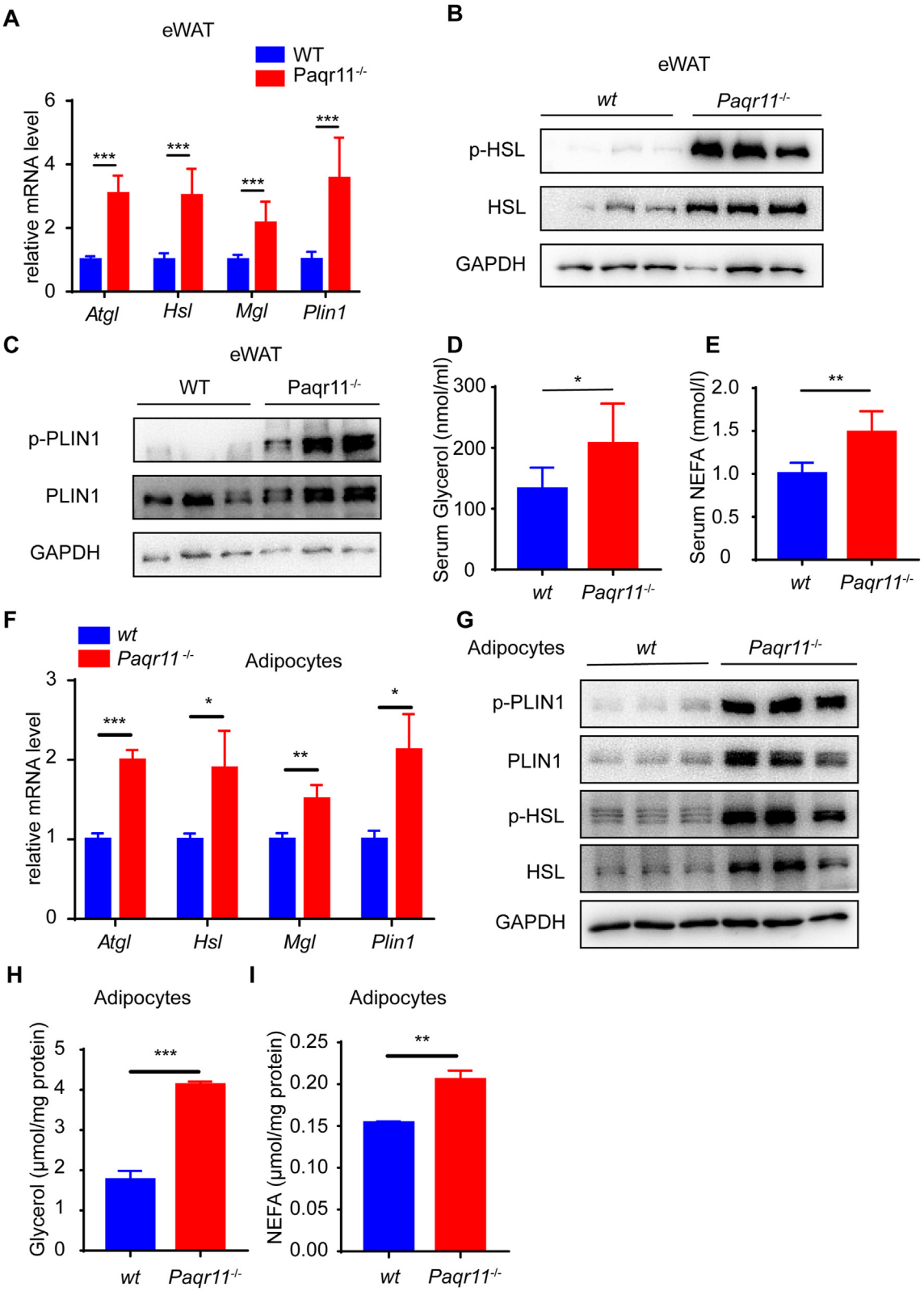

Figure 2: Deletion of *Paqr11* increases lipolysis in eWAT and adipocytes. (A) Quantitative RT-PCR analysis of lipolytic genes in eWAT of wild-type (*wt*) and *Paqr11*$^{-/-}$ male mice fed with HFD for 12 weeks (n = 8 for each group). The mice were fasted overnight before analysis. (B,C) Immunoblotting to detect the levels of phosphorylated HSL (p-HSL), total HSL, phosphorylated PLIN1 (p-PLIN1), and total PLIN1 in eWAT of the mice as in A using the antibodies as indicated. (D, E) Serum glycerol and non-esterized fatty acid (NEFA) levels of the mice as in A. (F) The mRNA levels of lipolytic genes in adipocytes differentiated from mouse embryonic fibroblasts (MEFs) of the mice as determined by quantitative real-time PCR. (G) Immunoblotting of P-HSL, HSL, p-PLIN1, and PLIN1 using the protein isolated from the adipocytes differentiated from MEFs. (H, I) Glycerol and NEFA levels in culture medium of the adipocytes as in G. All the quantitative data are shown as mean ± SD. * for $P < 0.05$, ** for $P < 0.01$, *** for $P < 0.001$.

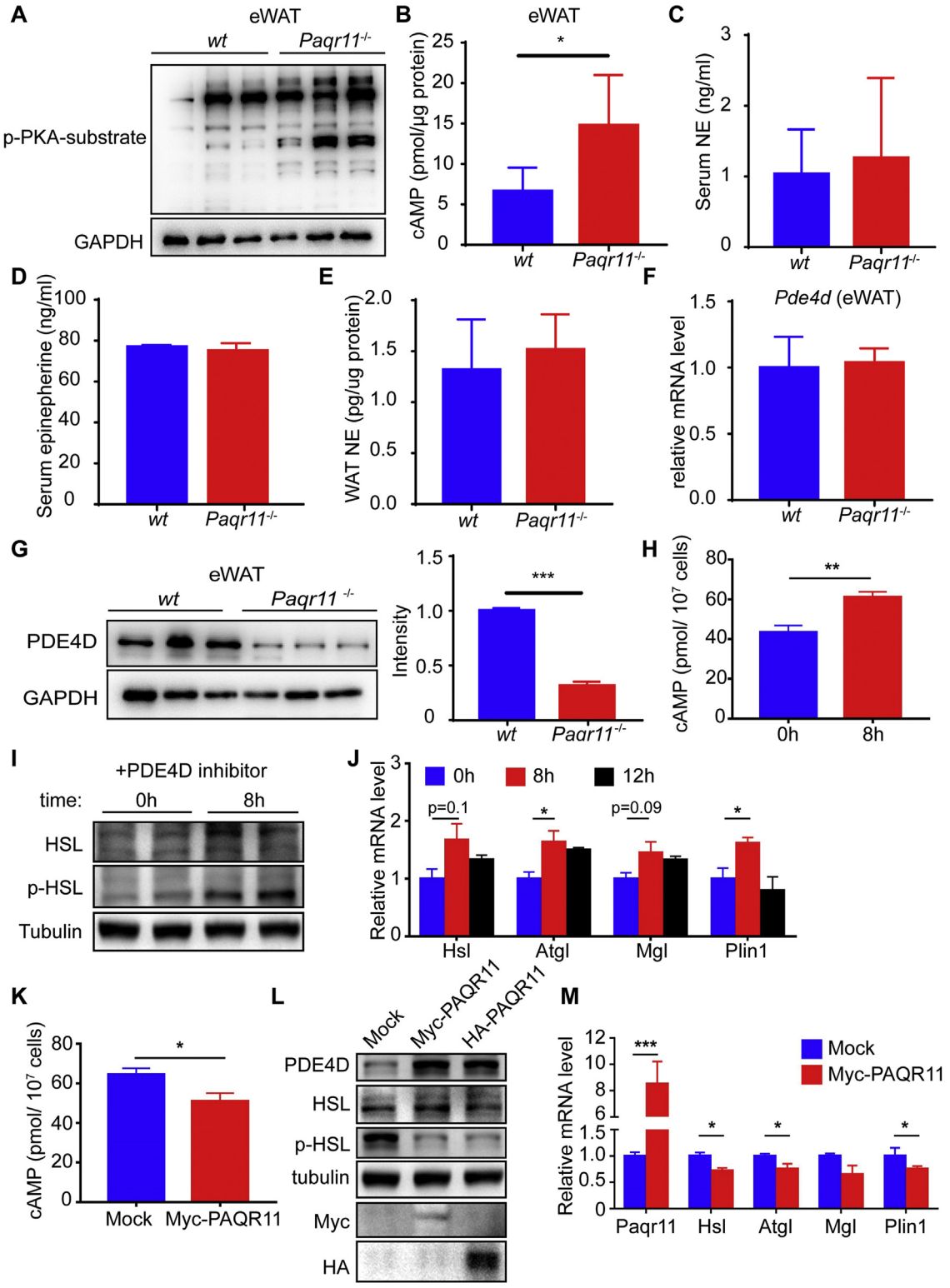

Figure 3: Deletion of *Paqr11* activates cAMP-PKA pathway and reduces PDE4D protein level. (A) Phosphorylated PKA substrates in total protein extracts of eWAT of wild-type (*wt*) and *Paqr11*$^{-/-}$ male mice fed with HFD for 12 weeks was analyzed by immunoblotting using the antibodies as indicated. The mice were fasted overnight before analysis. (B) The level of cAMP in eWAT of the mice as in A (n = 8 for each group). (C, D) Serum levels of norepinephrine (NE) and epinephrine (Epi) analyzed by ELISA with the mice as in A. (E) NE level in eWAT of the mice as in A. (F) Quantitative RT-PCR to detect the mRNA level of *Pde4d* in eWAT of the mice as in A. (G) PDE4D protein level analyzed by immunoblotting with eWAT of the mice as in A. The relative density of the protein bands is shown in the right panel. (H–J) The adipocytes differentiated from MEFs were treated with 1 μM of D159687 for various times and then used in measurement of cAMP level (for H), Western blotting (for H) and quantitative RT-PCR (for J). (K–M) The adipocytes differentiated from MEFs were overexpressed with PAQR11 and used in measurement of cAMP level (for K), Western blotting (for L) and quantitative RT-PCR (for M). All the quantitative data are shown as mean ± SD. * for $P < 0.05$, ** for $P < 0.01$, *** for $P < 0.001$.

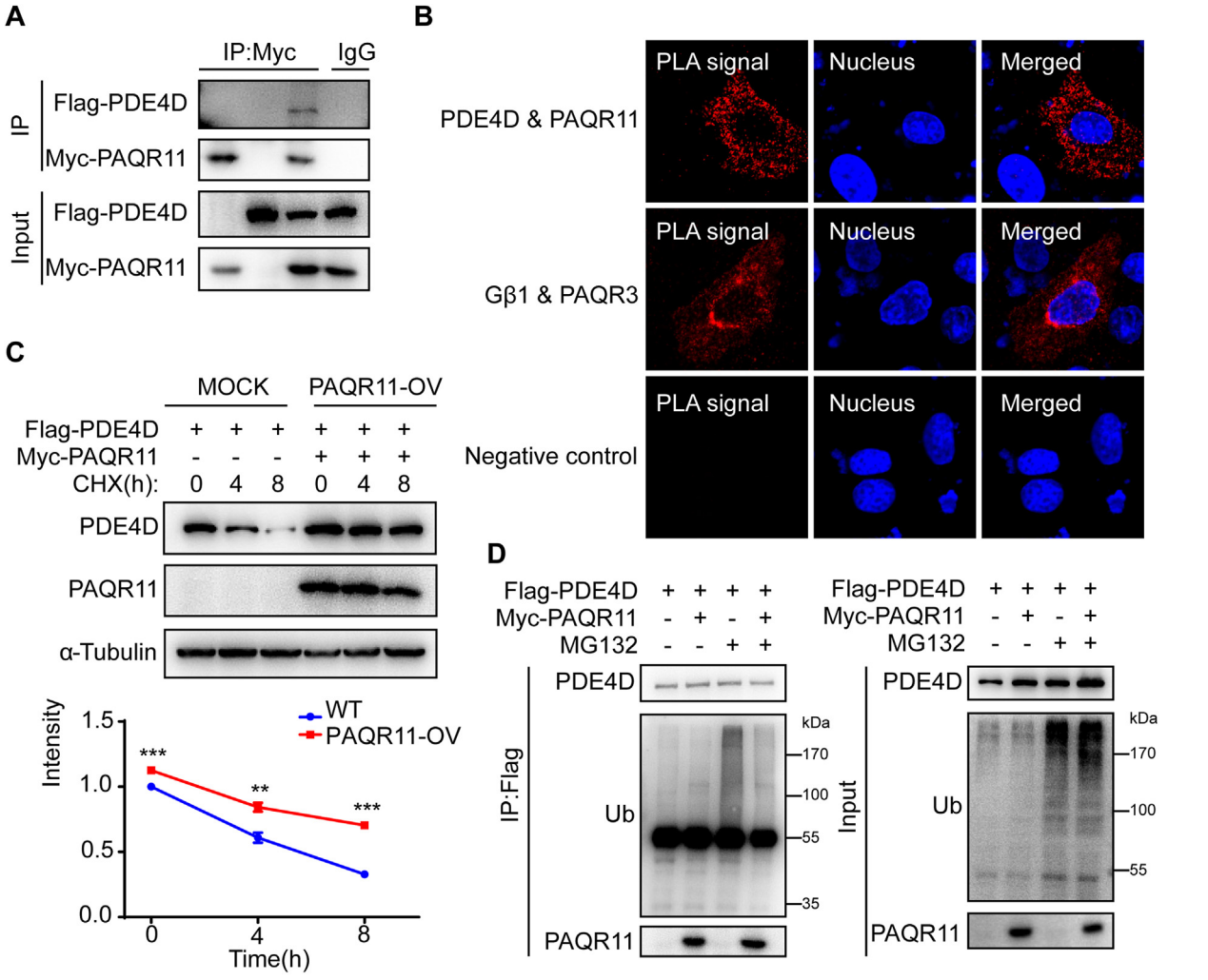

Figure 4: PAQR11 interacts with PDE4D and accelerates its degradation. (A) Co-immunoprecipitation of PAQR11 with PDE4D. HEK293T cells were transfected with the plasmids as indicated, followed by immunoprecipitation (IP) and immunoblotting (IB) with the antibodies as indicated. (B) Interaction of PAQR11 and PDE4D using Duolink PLA. Hela cells were co-transfected with Myc-tagged PAQR11, GFP-fused PDE4D, GFP-fused PAQR3, and Flag-tagged Gβ1 as indicated. PLA signals are shown in red, and there was no primary antibody for negative control which was over-expressing PAQR11 and PDE4D. (C) PAQR11 modulates the protein half-life of PDE4D. HEK293T cells were transfected with the plasmids as indicated and treated with cycloheximide (CHX) for various times. The cell lysate was used in immunoblotting with the antibodies as indicated. Quantitative measurement of PDE4D protein is shown in the lower panel (mean ± SD, ** for $P < 0.01$ and *** for $P < 0.001$ and ns for non-significant). The same experiments were repeated three time with similar results. (D) PAQR11 overexpression decreases poly-ubiquitination of PDE4D. HEK293T cells were transfected with the plasmids as indicated. The cells were pretreated with MG132 (10 μM) for 6 h, followed by IP and IB with the antibodies as indicated.

lipid metabolism especially lipolysis in eWAT together with an increase of browning in iWAT. These changes in white adipose tissues were consistent with an increased metabolic rate and reduced body weight in *Paqr11*-deleted mice.

2.3. Deletion of *Paqr11* elevates cAMP-PKA pathway and reduces PDE4D protein level

As PKA plays a key role in regulating the lipolysis program in adipose tissue [2,3], we analyzed the activity of PKA in our samples. The protein level of phosphorylated PKA (p-PKA) substrate, an index of PKA activity, was highly increased in eWAT of the *Paqr11*$^{-/-}$ mice compared to eWAT of the wild-type mice (Figure 3A). The cAMP level was also significantly increased in eWAT of the *Paqr11*$^{-/-}$ mice (Figure 3B), while it was not altered by *Paqr11* deletion in iWAT and BAT (SFigure 5). As sympathetic activation is a crucial factor in stimulating lipolysis via catecholamine-mediated activation of β-adrenergic receptors [10,19], we analyzed whether the catecholamine level was altered by *Paqr11* deletion. To our surprise, the serum levels of norepinephrine and epinephrine were not changed (Figure 3C and D). The norepinephrine level in the eWAT was also not changed (Figure 3E). These results indicated that the increase of lipolysis in the *Paqr11*-deleted adipose tissue is not likely caused by activation of the sympathetic system in the mice, but rather by a local mechanism. As the cAMP level was increased by *Paqr11* deletion (Figure 3B), we reasoned that a mechanism that modulates cAMP level might contribute to the change of lipolysis in the *Paqr11*$^{-/-}$ mice. As it was previously reported that PDE4D is involved in the regulation of cAMP level in adipose tissue [20], we analyzed the protein level and mRNA level of PDE4D. Interestingly, only the protein level but not the mRNA level of PDE4D was significantly reduced by *Paqr11* deletion (Figure 3F and G).

To provide additional evidence that PDE4D is involved in the regulation of lipolysis in adipocytes, we analyzed the effect of a selective PDE4D

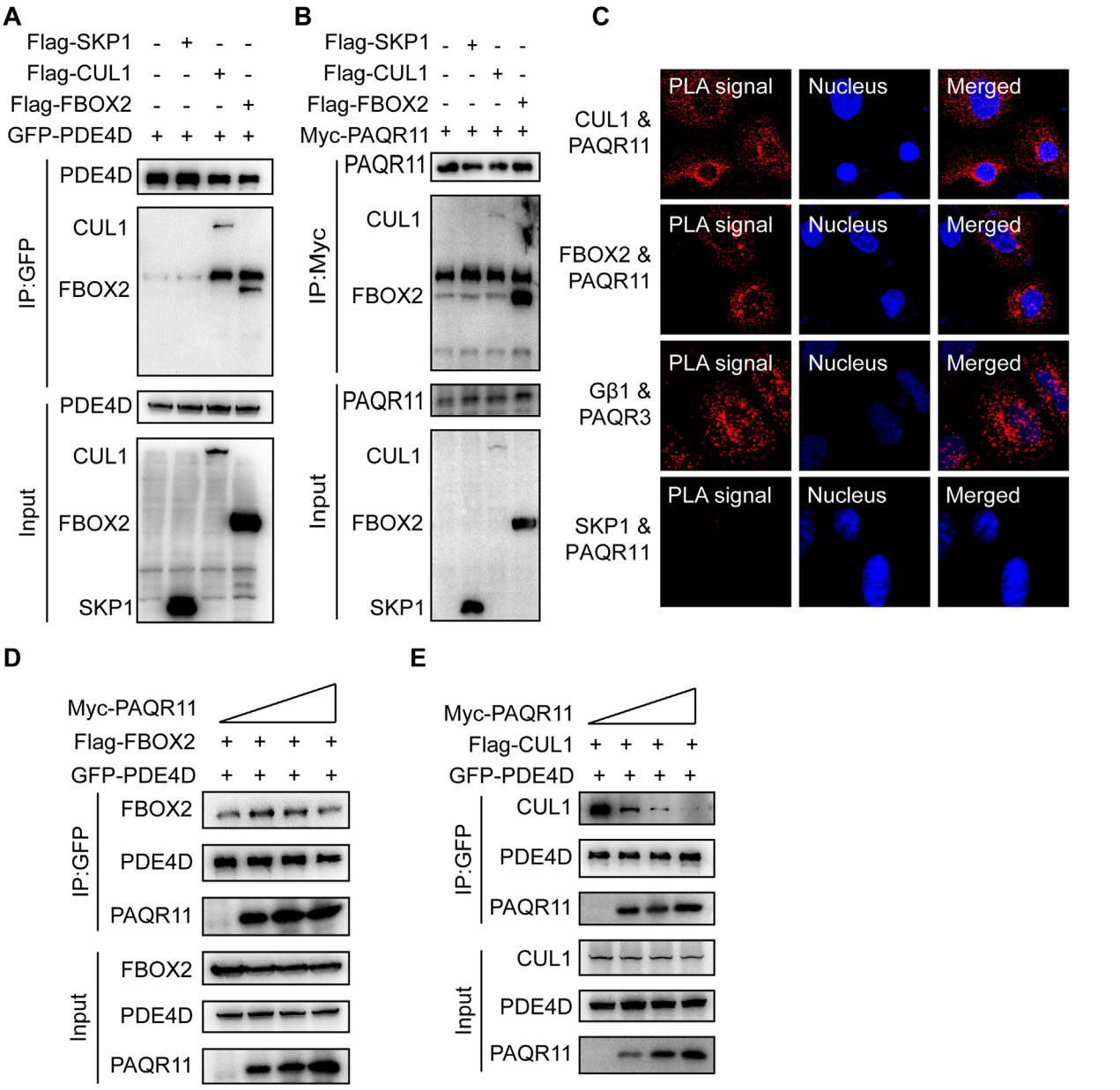

Figure 5: PAQR11 interacts with SKP1-CUL1-FBXO2 complex to regulate PDE4D degradation. (A) Co-immunoprecipitation of PDE4D with CUL1 and FBOX2. HEK293T cells were transfected with the plasmids as indicated, followed by immunoprecipitation (IP) and immunoblotting (IB) with the antibodies as indicated. (B) Co-immunoprecipitation of PAQR11 with CUL1 and FBOX2. HEK293T cells were transfected with the plasmids, followed by IP and IB. (C) Detection of PAQR11-CUL1 and PAQR11-FBOX2 interactions by Duolink PLA. Hela cells were co-transfected with Myc-tagged PAQR11 with Flag-tagged CUL1 (the first panel), Myc-tagged PAQR11 with Flag-tagged FBOX2 (the second panel), GFP-fused PAQR3 with Flag-tagged Gβ1 (the third panel), and Myc-tagged PAQR11 with Flag-tagged SKP1 (the fourth panel). PLA-positive signals are shown in red. (D, E) PAQR11 reduces the interaction of PDE4D with CUL1, but not PDE4D with FBOX2. HEK293T cells were transfected with the plasmids as indicated, followed by IP and IB.

inhibitor D159687 in adipocytes. We found that the PDE4D inhibitor could increase the intracellular cAMP level (Figure 3H), enhance HSL phosphorylation (Figure 3I), and elevate the expression of lipolysis-related genes (Figure 3J) in adipocytes differentiated from MEFs of the wild-type mice. In addition, PAQR11 overexpression could reduce cAMP level (Figure 3K), increase PDE4D protein level (Figure 3L), reduce HSL phosphorylation (Figure 3L), and reduce the expression of lipolysis-related genes (Figure 3M) in adipocytes differentiated from MEFs. Collectively, these results indicated that PAQR11-regulated PDE4D modulates lipolysis in eWAT as well as adipocytes via changes of lipolysis gene expression and cAMP-mediated lipolysis activity.

2.4. PAQR11 interacts with PDE4D and promotes its degradation via SKP1-CUL1-FBXO2 complex

As PAQR11 could modulate the protein level of PDE4D, we postulated that PAQR11 might physically interact with PDE4D. Consistent with our hypothesis, a co-immunoprecipitation experiment in HEK293T cells revealed that PAQR11 could associate with PDE4D (Figure 4A). To confirm the interaction of PAQR11 with PDE4D, we performed a proximity ligation assay (PLA), a method that allows both visualization and quantification of protein interactions when the two proteins are closer than 40 nm in spatial distance. As a positive control, PLA revealed a positive result (Figure 4B, middle panel) with the interaction

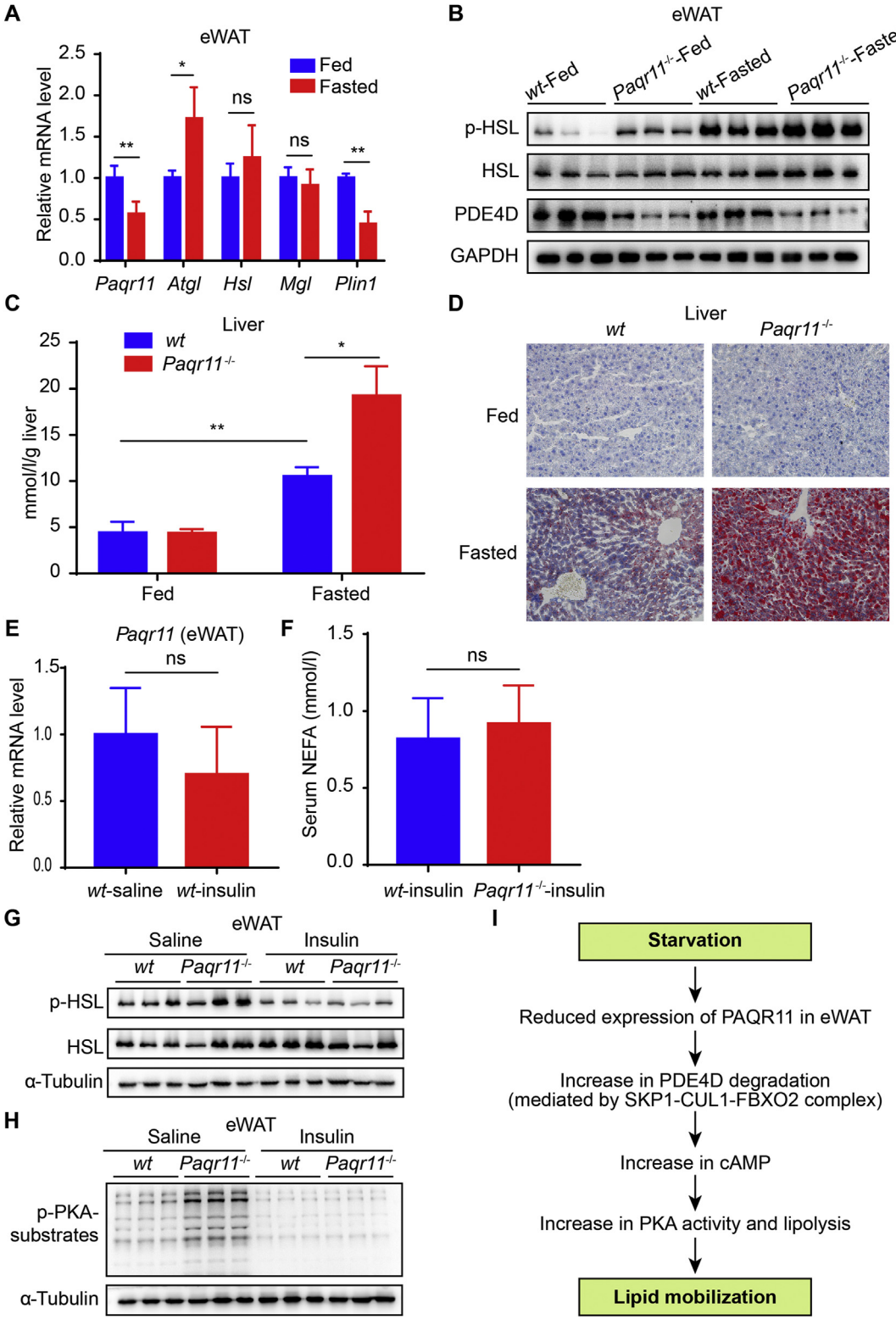

Figure 6: PAQR11 regulated fasting-induced lipolysis in eWAT and lipid accumulation in liver. (A) The mRNA levels of *Paqr11* and lipolytic genes in eWAT of wild-type mice at 12 weeks old fed with normal chow under fed and fasted (for 24 h) conditions as determined by quantitative RT-PCR. (B) Immunoblotting analyses of lipolytic proteins using eWAT from wild type (*wt*) and Paqr11$^{-/-}$ mice at 12 weeks old fed with normal chow under fed and fasted (for 24 h) conditions. (C) Liver triglyceride levels of the mice as in B. (D) Representative images of Oil Red O staining of the liver sections of the mice as in B. (E) The mRNA level of *Paqr11* in eWAT of saline—or insulin-injected wild-type mice. Insulin was used at 0.6 U/kg. (F) Serum level of non-esterized fatty acid (NEFA) of the saline—or insulin-injected 12-week-old *wt* and Paqr11$^{-/-}$ mice fed with normal chow. (G) Immunoblotting to analyze phosphorylated HSL and total HSL of the mice as in F. (H) Immunoblotting to detect phosphorylated PKA substrates of the mice as in F. (I) A diagram to depict the working model of PAQR11 regulation on fasting-induced lipolysis in adipose tissue. All the quantitative data are shown as mean ± SD. * for $P < 0.05$, ** for $P < 0.01$, *** for $P < 0.001$ and ns for non-significant.

of PAQR3 with G protein β1 subunit (Gβ1) as reported previously [21]; there was no red spot signal with the negative control (Figure 4B, the lower panel). Notably, the interaction between PAQR11 and PDE4D was found by PLA (Figure 4B, upper panel). We next investigated whether PAQR11 could regulate the protein stability of PDE4D. We analyzed the half-life of PDE4D protein in HEK293T cells by treating the cells with cycloheximide to stop synthesis of new proteins. Overexpression of PAQR11 slowed down the degradation rate of PDE4D protein (Figure 4C). To determine whether PAQR11 could affect the proteasome-mediated degradation of PDE4D protein, we analyzed PDE4D protein polyubiquitination levels in the presence or absence of MG132, a proteasome inhibitor. In the presence of MG132, PDE4D polyubiquitination levels were reduced by PAQR11 overexpression in HEK293T cells (Figure 4D).

It was previously reported that PDE4D could be degraded by the ubiquitin-dependent proteasome pathway through and Cullin 1 (CUL1)-containing SKP1-CUL1-FBXO2 (SCF) E3 ubiquitin ligase complex or MDM2 [22,23]. We found that PAQR11 overexpression had no effect on the PDE4D ubiquitination promoted by MDM2 (SFigure 6). We next analyzed whether PDE4D degradation was mediated by the SKP1-Cullin-Fbox complex that mediates polyubiquitination and degradation of numerous proteins [24]. Using a co-immunoprecipitation assay, we found that both PDE4D and PAQR11 could interact with CUL1 and FBXO2, but not SKP1 (Figure 5A and B). The interactions of PAQR11 with CUL1 and FBXO2 were also confirmed by proximity ligation assay (Figure 5C, the first two panels). As a positive control, PAQR3 was co-localized with G protein β1 subunit as previously reported (Figure 5C, the third panel) [21]. As a negative control, SKP1 was not co-localized with PAQR11 (Figure 5C, the fourth panel). We next analyzed how PAQR11 affected the interaction of PDE4D with the components of the SCF complex. We found that PAQR11 had no significant effect on the interaction between PDE4D and FBXO2 (Figure 5D). However, PAQR11 could dose-dependently reduce the interaction between PDE4D and CUL1 (Figure 5E). Taken together, these results indicated that PAQR11 may antagonize SKP1-CUL1-FBXO2-mediated degradation of PDE4D via competing for binding with CUL1, thus leading to reduced degradation of PDE4D protein.

2.5. PAQR11 regulates fasting-induced lipolysis in adipose tissue and lipid accumulation in the liver

As the physiological function of lipolysis of adipose tissue is mainly to provide energy during starvation, we next investigated whether PAQR11 modulated this process. We first examined the mRNA level of *Paqr11* under both fed and fasting conditions. Intriguingly, the mRNA level of *Paqr11* was significantly reduced under fasting conditions (Figure 6A). Consistently, starvation also reduced *Paqr11* expression in adipocytes differentiated from MEFs (SFigure 7). HFD did not alter the Paqr11 expression in the adipose tissue (SFigure 8). As expected, phosphorylation of HSL in eWAT was increased by fasting (Figure 6B). Moreover, the fasting-induced increase in HSL phosphorylation was augmented by deletion of *Paqr11* (Figure 6B), indicating that PAQR11 has a negative effect on starvation-induced lipolysis in adipose tissue. In addition to stimulation of lipolysis in adipose tissue, starvation is known to cause a transient lipid accumulation in the liver due to an increase in fat mobilization. As expected, fasting was able to robustly increase the liver triglyceride (TG) level (Figure 6C). *Paqr11* deletion further enhanced the elevation of TG level in the liver (Figure 6C). Consistently, Oil Red O staining of the liver sections demonstrated that the *Paqr11* deletion aggravated fasting-mediated lipid accumulation in the liver (Figure 6D). These findings, therefore, indicate that PAQR11 is involved in fasting-induced lipolysis in adipose tissue and lipid accumulation in the liver.

During the feeding—fasting cycle, insulin is known to play a crucial role in negatively regulating lipolysis of adipose tissue upon feeding [2,3]. We next analyzed whether PAQR11 could modulate insulin-mediated suppression of lipolysis. The mice were fasted overnight, and insulin was administered afterward. The mRNA level of *Paqr11* was not affected by insulin treatment (Figure 6E). The serum FFA level did not differ between the wild-type mice and the *Paqr11*-deleted mice (Figure 6F). Furthermore, the insulin-mediated inhibitions on HSL phosphorylation and phosphorylated PKA substrate level were not affected by *Paqr11* deletion (Figure 6G and H), indicating that insulin-mediated suppression of lipolysis in adipose tissue is not affected by PAQR11. In other words, these results suggested that PAQR11 mainly regulates lipolysis under the fasting condition, but not under the feeding condition in which insulin plays a dominant role to suppress lipolysis.

3. DISCUSSION

Our study reveals a new mechanism that aids in comprehending how lipolysis in adipose tissue is regulated by starvation. As illustrated (Figure 6I), fasting reduces the expression of Paqr11. The decreased PAQR11 relieves its inhibitory effect on the interaction of PDE4D with SCF complex, a E3 ubiquitin ligase, thus leading to enhancement of polyubiquitination and degradation of PDE4D. The decrease in PDE4D protein subsequently results in accumulation of cAMP and elevation of PKA activity, thereby enhancing the lipolysis program in adipose tissue. Previously, a number of theories have been proposed to explain the underlying mechanism of lipolysis regulation by starvation [2,3]. The mainstream view is that the sympathetic nervous system is activated by starvation [5,10,25]. However, there is little evidence showing that the systemic or local level of catecholamines is increased by starvation. A few studies have indicated that the sensitivity of adipose tissue to catecholamines is enhanced under fasting conditions [25]. Therefore, our study provides new insight on how starvation enhances lipolytic sensitivity of adipose tissue.

Our study also pinpoints that different adipose tissues respond to physiological situations differently in terms of lipid mobilization, as we only observed a significant regulation of lipolysis in eWAT by PAQR11. In humans, numerous studies have explored the differential contribution of differently located fat tissues to obesity as well as differential response, including lipid uptake and lipid mobilization, to diet and exercise [2,26,27]. However, there were few studies in animal models to decipher the differential involvement of different fat tissues in lipid mobilization. Our results are partly consistent with the studies by Bartness' group using Siberian hamsters. When Siberian hamsters are transferred from long summer-like days (LDs) to short winter-like days (SDs), the adiposity of the animals is reduced. It was found that SDs induces a greater decrease in eWAT than iWAT, together with an increased norepinephrine turnover rate in eWAT, indicating a greater innervation of sympathetic nervous system in eWAT than iWAT [28]. Based on the results of Bartness' study, we postulate that *Paqr11* deletion has a stronger effect in eWAT than iWAT as eWAT likely has a greater innervation of sympathetic nervous system than iWAT. As our study demonstrated for the first time that starvation-induced lipolysis is differentially regulated by PAQR11 in different adipose tissues, our finding would aid in clarifying the important physiological question about how different adipose tissues are differentially regulated during the feeding/starvation cycle.

Our study also demonstrates a close link between regulation of lipolysis and metabolic homeostasis. Obesity, mainly manifested as accumulation of TG in adipose tissue, can be attained through two major mechanisms, *i.e.*, enhanced lipogenesis due to extra energy intake and reduced lipolysis during starvation. An increase in "basal" lipolysis, as observed in *Paqr11*-deleted mice, results in significant reduction in body weight. In particular, the HFD-induced obesity was markedly reduced by *Paqr11* deletion (Figure 1D). It is noteworthy that in most studies, a reduction in obesity is always associated with improvement in glucose metabolism. However, in our study, glucose tolerance and insulin sensitivity were not altered in HFD-fed *Paqr11*$^{-/-}$ mice (SFigure 2F and G). Such observation clearly indicates that an improvement of obesity is not necessarily associated with an improvement in glucose homeostasis. We propose that lipolysis in adipose tissue mainly impacts lipid accumulation and obesity in the body, but not on glucose metabolism.

In general, activation of the sympathetic system and the downstream adrenergic receptors in adipose tissue can stimulate both lipolysis and thermogenesis [29]. To our surprise, we found that *Paqr11* deletion did not alter cold-induced UCP1 expression in BAT (data not shown). These data indicate that lipolysis and thermogenesis can be dissociated. One possibility is that activation of adrenergic receptors by itself is not sufficient to turn on lipolysis and thermogenesis in adipose tissue and other factors/molecules are needed. As PAQR11 mainly modulates lipolysis process in adipose tissue, we postulate that PAQR11 may do this by regulating other factors/molecules in addition to the adrenergic receptor-AC-cAMP-PKA pathway.

The Skp1-Cul1-Fbox (SCF) complex is involved in polyubiquitination and degradation of numerous proteins and affects many biological processes, especially cell growth [24]. Our study has added to the list of proteins regulated by the SCF complex. Within the SCF complex, Cul1 is a scaffold that brings together Skp1 and Fbox proteins. Skp1 is an adaptor that links the Fbox substrate-specific factor to the ligase complex. Fbox is the E3 ligase of the complex and recognizes specific substrates, subsequently leading to polyubiquitination and degradation of the substrates. There are 69 Fbox-encoding genes in humans, and different Fbox proteins are involved in degradation of different sets of proteins [24]. In our study, we found FBXO2 of the SCF complex is involved in the degradation of PDE4D, and the interaction of SKP1-CUL1-FBXO2 complex with PDE4D is antagonized by PAQR11. *Fbxo2* was shown to be highly expressed in the brain and cochlea, and deletion of *Fbxo2* was found to affect neuronal connectivity and cochlear development [30,31]. It remains to be determined whether FBXO2 also affects lipolysis in adipose tissue.

In summary, our study indicated that the major physiological function of PAQR11 *in vivo* is regulating starvation-induced lipolysis in adipose tissue. Our study also revealed that regulation of lipolysis in adipose tissue is closely associated with the development of obesity without affecting glucose homeostasis. Furthermore, we revealed that PDE4D in adipose tissue is involved in modulating adrenergic receptor activation-induced lipolysis, indicating that PDE4D could be a potential target for control of lipolysis and obesity [32]. It is worth noting that many isoforms of PDEs are expressed in the adipose tissues, and thus we cannot rule out the possibility that other PDEs are involved in the regulation of lipolysis. In addition, *Paqr11* deletion might alter the movement of the mice (Figure 1K and L), likely contributing to the reduced body weight in *Paqr11*$^{-/-}$ mice. On the other hand, *Paqr11* was found to be highly expressed in the brain (Figure 1A). We could not rule out the possibility that PAQR11 may regulate energy metabolism via altering brain functions or behavior. Nevertheless, our study provides a new insight to comprehend the complex regulation of lipolysis in adipose tissue. Such study can also aid in future combat against obesity, one of the most common modern diseases.

4. MATERIALS AND METHODS

4.1. Materials and antibodies

The materials and antibodies used in this study were purchased as follows: anti-HSL from Cell Signaling Technology (4107s, Danvers, MA, USA); anti-phospho-HSL (Ser660) from Cell Signaling Technology (4126s); anti-phospho-PKA substrate from Cell Signaling Technology (9621s); Anti-GAPDH from ABclonal (AC033, Boston, MA, USA); anti-Flag tag from Sigma—Aldrich (F3165, St. Louis, MO, USA); anti-GM130 from Abcam (ab52649, Cambridge, UK); anti-PDE4D from Abcam (ab14613); anti-perilipin1 from Vala Sciences (4854, San Diego, CA, USA); anti-p-perilipin1 from Vala Sciences (4856); anti-α-tubulin from Sigma—Aldrich (T6199); anti-Myc tag from Santa Cruz Biotechnology (sc-40, Santa Cruz, CA); anti-GFP from Santa Cruz Biotechnology (sc-9996); cycloheximide (CHX) and polyethylenimine (PEI) from Sigma—Aldrich (C7698); Alexa Fluor 546 goat anti-mouse IgG from Abcam (A11003); Alexa Fluor 546 goat anti-rabbit IgG from Abcam (A11035); Alexa Fluor 488 goat anti-mouse IgG from Abcam (A11029); Alexa Fluor 488 goat anti-rabbit IgG from Abcam (A11034). The selective PDE4D inhibitor D-159687 (CSN23886) was from CSNpharm (Chicago, MI, USA).

4.2. Animal studies

The *Paqr11* knockout mice were developed in the Model Animal Research Center of Nanjing University (Nanjing, Jiangsu, China). All animals were maintained and used in accordance with the guidelines of the Institutional Animal Care and Use Committee of the Shanghai Institute of Nutrition and Health, Chinese Academy of Sciences with an approval number 2010-AN-8. Mice were maintained on a 12-h light/dark cycle at 25 °C. Homozygous Paqr11$^{-/-}$ mice in C57BL/6J background were generated by crossing with the C57BL/6J strain for at least six generations.

4.3. Plasmid construction

The Myc-tagged Paqr11 was generated by polymerase chain reaction (PCR) using human *Paqr11* plasmids as previously reported [17]. Flag-tagged Skp1, Flag-tagged Cullin1 and Flag-tagged Fbxo2 were generated by PCR using cDNA isolated from HEK293T cells and cloned into pLVXm-N-flag-IRES-Puro vector with confirmation by DNA sequencing. PDE4D cDNA was purchased from LncBio Co. (NM_001197222, Shanghai, China). The Flag-tagged PDE4D was generated by PCR using human PDE4D plasmid and cloned into pLVXm-N-flag-IRES-Puro vector with confirmation by DNA sequencing. The GFP-tagged PDE4D was generated by PCR using human PDE4D plasmid and cloned into pEGFP-C1 vector.

4.4. Cell culture and transfection

HEK293T and Hela cell lines were cultured in completed medium consisting of Dulbecco's modified Eagle's medium (DMEM) containing 10% fetal bovine serum (FBS), and 1% penicillin-streptomycin at 37 °C with 5% CO_2. Transient transfection was performed with the polyethylenimine (PEI) (Sigma—Aldrich) method for HEK293T cells. Transfection in Hela cells was performed using PolyJet transfection reagents (Signagen Laboratories, Rockville, MD, USA).

4.5. Co-immunoprecipitation, immunoblotting, and immunofluorescence staining

The methods of cell lysis, co-immunoprecipitation, immunoblotting, immunostaining, and confocal microscopy analysis were performed as previously reported [33]. Nuclei were stained with Hoechst 33,342 (Molecular Probes, H-3570).

4.6. MEF isolation and differentiation

MEF isolation was performed according to previously described methods [33,34]. Primary mouse embryonic fibroblasts (MEFs) were isolated from 12.5 to 14.5 pregnant heterozygous *Paqr11*-deleted mice. Wildtype or *Paqr11*$^{-/-}$ MEFs were differentiated into adipocytes by a standard protocol. Briefly, differentiation was induced 2 days post confluency by addition of DMEM containing 10% FBS and dexamethasone (0.25 μM), 3-Isobutyl-1-methylxanthine IBMX (0.5 μM), insulin (1 mg/ml), and rosiglitazone (20 μM) for 4 days. The cells were further incubated with DMEM/FBS supplemented with insulin and rosiglitazone for 4–6 days with medium change every two days.

4.7. Measurement of norepinephrine, epinephrine, and cAMP

Commercial enzyme-linked immunosorbent assay (ELISA) kits were used to measure norepinephrine (NE) (CEA907Ge, Cloud-Clone Corp, Houston, TX, USA), epinephrine (CEA858Ge, Cloud-Clone Corp) and cAMP (R&D Systems, KGE012B, Minneapolis, USA), according to the manufacturer's instructions.

4.8. Lipolysis assays

Commercial FFA measurement kit (Wako Chemicals, Osaka, Japan) and glycerol assay kits (ab 65,337) were used for measuring FFA and glycerol levels in the serum and cell culture medium according to the manufacturer's instructions.

4.9. RNA isolation and real-time PCR

Total RNA of cells and tissues were lysed by TRIzol reagent (Invitrogen, Carlsbad, CA, USA) and purified according to manufacturer's instructions. RNA was reverse transcribed with a high-capacity cDNA reverse transcription kit (Tiangen, Shanghai, China). Gene expression was determined by reverse transcription PCR (RT-PC)R performed with an ABI 7900 system (Applied Biosystems). The primers used in real-time PCR were as follows: 5′-GATCATTGCTCCTCCTGAGC-3′ and 5′-ACTCCTGCTTGCTGATCCAC-3′ for mouse β-actin; 5′-CAGCTAATGGCCGCTACAAAC-3′ and 5′-CAGCAGTCATCAGACAGCCG-3′ for mouse *Paqr11*; 5′-CAGCACATTTATCCCGGTGTAC-3′ and 5′-AAATGCCGCCATCCACATAG-3′ for mouse *Atgl*; 5′-GCTGGAGGAGTGTTTTTTTGC-3′ and 5′-AGTTGAACCAAGCAGGTCACA-3′ for mouse *Hsl*; 5′-AGGCGAACTCCACAGAATGTT-3′ and 5′-ACAAAAGAGGTACTGTCCGTCT-3′ for mouse *Mgl*; 5′-CTGTGTGCAATGCCTATGAGA-3′ and 5′-CTGGAGGGTATTGAAGAGCCG-3′ for mouse *Plin1*; 5′-TTTTGCCAGTGCAATACATGATG-3′ and 5′-CAGAGCGAGTTCCGAGTTTGT-3′ for mouse *Pde4d*. The reference gene for RT-PCR was β-actin.

4.10. Metabolic phenotyping and staining with hematoxylin and eosin (H&E)

^{1}H-nuclear magnetic resonance (NMR) spectroscopy was used to measure fat and lean mass of the mice. A comprehensive laboratory animal monitoring system (Columbus Instruments) was used to monitor metabolic rate and physical activity according to the manufacturer's instructions. For glucose tolerance tests (GTT), mice fasted overnight were injected with glucose at 1 g/kg body weight. For insulin tolerance tests (ITT), mice fasted for 4–6 h before intraperitoneal injection of insulin (Roche, Basel, Switzerland) at 1 U/kg body weight. Glucose concentrations were measured at 0, 15, 30, 60, 90, and 120 min after injection. Alanine aminotransferase (ALT), aspartate aminotransferase (AST), TG, TC, HDL-C, and LDL-C were measured by the assay kits from ShenSuoYouFu (Shanghai, China). The concentrations of liver TG were normalized to protein concentrations. H&E staining was performed by Servicebio (Shanghai, China).

4.11. Duolink in situ proximity ligation assay (PLA)

PLA was performed with a kit purchased from Sigma–Aldrich [35]. Hela cells seeded on coverslips in 12-well plates were transfected with different plasmids. At 24 h post transfection, the cells were fixed with 4% paraformaldehyde for 5 min, washed with phosphate-buffered saline (PBS), and then permeabilized with 0.1% Triton X-100 in PBS for 5 min at room temperature. PLA was then performed by following the manufacturer's instructions.

4.12. Statistical analysis

Student's t-test was used to analyze the data. P value < 0.05 was considered statistically significant, and all results were expressed as mean ± standard deviation (SD).

AUTHOR CONTRIBUTION

Y.C. conceptualized the study. M.H. and Y.C. designed the study and wrote the paper. M.H. and Y.L. performed the experiments. L.W., X.Y., S.W., J.Z., M.B., and Z.L. provided technical assistance.

ACKNOWLEDGMENT

This study was supported by research grants from the National Natural Science Foundation of China (31630036to Y.C.), the Ministry of Science and Technology of China (2016YFA0500103to Y.C.), and the Chinese Academy of Sciences (XDA12010102, QYZDJ-SSW-SMC008, ZDRW-ZS-2016-8, and Y817X11141 to Y.C.).

CONFLICT OF INTEREST

None declared.

APPENDIX A. SUPPLEMENTARY DATA

Supplementary data to this article can be found online at https://doi.org/10.1016/j.molmet.2021.101182.

REFERENCES

[1] Soeters, M.R., Soeters, P.B., Schooneman, M.G., Houten, S.M., Romijn, J.A., 2012. Adaptive reciprocity of lipid and glucose metabolism in human short-term starvation. American Journal of Physiology. Endocrinology and Metabolism 303(12):E1397–E1407.

[2] Arner, P., Langin, D., 2014. Lipolysis in lipid turnover, cancer cachexia, and obesity-induced insulin resistance. Trends in Endocrinology and Metabolism 25(5):255–262.

[3] Zechner, R., Madeo, F., Kratky, D., 2017. Cytosolic lipolysis and lipophagy: two sides of the same coin. Nature Reviews Molecular Cell Biology 18(11):671–684.

[4] Kopelman, P.G., 2000. Obesity as a medical problem. Nature 404(6778):635–643.

[5] Zeng, W., Pirzgalska, R.M., Pereira, M.M., Kubasova, N., Barateiro, A., Seixas, E., et al., 2015. Sympathetic neuro-adipose connections mediate leptin-driven lipolysis. Cell 163(1):84–94.
[6] Bolsoni-Lopes, A., Alonso-Vale, M.I., 2015. Lipolysis and lipases in white adipose tissue - an update. Archives of Endocrinology and Metabolism 59(4): 335–342.
[7] Fruhbeck, G., Mendez-Gimenez, L., Fernandez-Formoso, J.A., Fernandez, S., Rodriguez, A., 2014. Regulation of adipocyte lipolysis. Nutrition Research Reviews 27(1):63–93.
[8] Wijkander, J., Landstrom, T.R., Manganiello, V., Belfrage, P., Degerman, E., 1998. Insulin-induced phosphorylation and activation of phosphodiesterase 3B in rat adipocytes: possible role for protein kinase B but not mitogen-activated protein kinase or p70 S6 kinase. Endocrinology 139(1):219–227.
[9] DiPilato, L.M., Ahmad, F., Harms, M., Seale, P., Manganiello, V., Birnbaum, M.J., 2015. The role of PDE3B phosphorylation in the inhibition of lipolysis by insulin. Molecular and Cellular Biology 35(16):2752–2760.
[10] Bartness, T.J., Liu, Y., Shrestha, Y.B., Ryu, V., 2014. Neural innervation of white adipose tissue and the control of lipolysis. Frontiers in Neuroendocrinology 35(4):473–493.
[11] Liljenquist, J.E., Bomboy, J.D., Lewis, S.B., Sinclair-Smith, B.C., Felts, P.W., Lacy, W.W., et al., 1974. Effects of glucagon on lipolysis and ketogenesis in normal and diabetic men. Journal of Clinical Investigation 53(1):190–197.
[12] Ho, K.Y., Veldhuis, J.D., Johnson, M.L., Furlanetto, R., Evans, W.S., Alberti, K.G., et al., 1988. Fasting enhances growth hormone secretion and amplifies the complex rhythms of growth hormone secretion in man. Journal of Clinical Investigation 81(4):968–975.
[13] Ceddia, R.B., 2013. The role of AMP-activated protein kinase in regulating white adipose tissue metabolism. Molecular and Cellular Endocrinology 366(2): 194–203.
[14] Lamming, D.W., Sabatini, D.M., 2013. A Central role for mTOR in lipid homeostasis. Cell Metabolism 18(4):465–469.
[15] Picard, F., Kurtev, M., Chung, N., Topark-Ngarm, A., Senawong, T., Machado De Oliveira, R., et al., 2004. Sirt1 promotes fat mobilization in white adipocytes by repressing PPAR-gamma. Nature 429(6993):771–776.
[16] Tang, Y.T., Hu, T., Arterburn, M., Boyle, B., Bright, J.M., Emtage, P.C., et al., 2005. PAQR proteins: a novel membrane receptor family defined by an ancient 7-transmembrane pass motif. Journal of Molecular Evolution 61(3):372–380.
[17] Jin, T., Ding, Q., Huang, H., Xu, D., Jiang, Y., Zhou, B., et al., 2012. PAQR10 and PAQR11 mediate Ras signaling in the Golgi apparatus. Cell Research 22(4):661–676.
[18] Tan, X., Banerjee, P., Guo, H.F., Ireland, S., Pankova, D., Ahn, Y.H., et al., 2017. Epithelial-to-mesenchymal transition drives a pro-metastatic Golgi compaction process through scaffolding protein PAQR11. Journal of Clinical Investigation 127(1):117–131.
[19] Kolditz, C.I., Langin, D., 2010. Adipose tissue lipolysis. Current Opinion in Clinical Nutrition and Metabolic Care 13(4):377–381.
[20] Meng, W., Liang, X., Chen, H., Luo, H., Bai, J., Li, G., et al., 2017. Rheb inhibits beiging of white adipose tissue via PDE4D5-dependent downregulation of the cAMP-PKA signaling pathway. Diabetes 66(5):1198–1213.
[21] Jiang, Y., Xie, X., Zhang, Y., Luo, X., Wang, X., Fan, F., et al., 2010. Regulation of G-protein signaling by RKTG via sequestration of the G betagamma subunit to the Golgi apparatus. Molecular and Cellular Biology 30(1):78–90.
[22] Zhu, H., Suk, H.Y., Yu, R.Y., Brancho, D., Olabisi, O., Yang, T.T., et al., 2010. Evolutionarily conserved role of calcineurin in phosphodegron-dependent degradation of phosphodiesterase 4D. Molecular and Cellular Biology 30(18): 4379–4390.
[23] Li, X., Baillie, G.S., Houslay, M.D., 2009. Mdm2 directs the ubiquitination of beta-arrestin-sequestered cAMP phosphodiesterase-4D5. Journal of Biological Chemistry 284(24):16170–16182.
[24] Lee, E.K., Diehl, J.A., 2014. SCFs in the new millennium. Oncogene 33(16): 2011–2018.
[25] Jensen, M.D., Haymond, M.W., Gerich, J.E., Cryer, P.E., Miles, J.M., 1987. Lipolysis during fasting. Decreased suppression by insulin and increased stimulation by epinephrine. Journal of Clinical Investigation 79(1):207–213.
[26] Bjorntorp, P., 1996. The regulation of adipose tissue distribution in humans. International Journal of Obesity and Related Metabolic Disorders 20(4):291–302.
[27] Votruba, S.B., Jensen, M.D., 2007. Regional fat deposition as a factor in FFA metabolism. Annual Review of Nutrition 27:149–163.
[28] Youngstrom, T.G., Bartness, T.J., 1995. Catecholaminergic innervation of white adipose tissue in Siberian hamsters. American Journal of Physiology 268(3 Pt 2):R744–R751.
[29] Mahu, I., Domingos, A.I., 2017. The sympathetic neuro-adipose connection and the control of body weight. Experimental Cell Research 360(1):27–30.
[30] Nelson, R.F., Glenn, K.A., Zhang, Y., Wen, H., Knutson, T., Gouvion, C.M., et al., 2007. Selective cochlear degeneration in mice lacking the F-box protein, Fbx2, a glycoprotein-specific ubiquitin ligase subunit. Journal of Neuroscience 27(19):5163–5171.
[31] Atkin, G., Moore, S., Lu, Y., Nelson, R.F., Tipper, N., Rajpal, G., et al., 2015. Loss of F-box only protein 2 (Fbxo2) disrupts levels and localization of select NMDA receptor subunits, and promotes aberrant synaptic connectivity. Journal of Neuroscience 35(15):6165–6178.
[32] Lugnier, C., Meyer, A., Talha, S., Geny, B., 2020. Cyclic nucleotide phosphodiesterases: new targets in the metabolic syndrome? Pharmacology & Therapeutics 208:107475.
[33] Feng, L., Xie, X., Ding, Q., Luo, X., He, J., Fan, F., et al., 2007. Spatial regulation of Raf kinase signaling by RKTG. Proceedings of the National Academy of Sciences of the USA 104(36):14348–14353.
[34] Qiu, L.Q., Lai, W.S., Stumpo, D.J., Blackshear, P.J., 2016. Mouse embryonic fibroblast cell culture and stimulation. Bio Protocol 6(13).
[35] Fredriksson, S., Gullberg, M., Jarvius, J., Olsson, C., Pietras, K., Gustafsdottir, S.M., et al., 2002. Protein detection using proximity-dependent DNA ligation assays. Nature Biotechnology 20(5):473–477.

